

## PARAMETRIC OPTIMISATION OF FRICTION STIR WELDING ON ALUMINIUM ALLOY (EN AW-1100) PLATES

MUHAMMAD UMER FAROOQ AWAN<sup>a</sup>, MAHMOOD KHAN<sup>b,c,\*</sup>, KHALID WAHEED<sup>a</sup>,  
ZAFAR IQBAL<sup>a</sup>, ABDUL REHMAN<sup>d,e</sup>, FAHAD ALI<sup>a</sup>, MUHAMMAD SHAHZAD<sup>e</sup>,  
MUHAMMAD ABDUL BASIT SAIM<sup>c</sup>, SHAHID AKHTAR<sup>f</sup>,  
RAGNHILD ELIZABETH AUNE<sup>b</sup>

<sup>a</sup> Pakistan Institute of Engineering and Applied Sciences, Department of Nuclear Engineering, Nilore, 45650, Pakistan

<sup>b</sup> Norwegian University of Science and Technology, Faculty of Natural Sciences, Department of Materials Science and Engineering, Trondheim, 7491, Norway

<sup>c</sup> Institute of Space Technology, Department of Materials Science and Engineering, Islamabad, 44000, Pakistan

<sup>d</sup> Pakistan Institute of Engineering and Applied Sciences, Department of Metallurgy and Materials Engineering, Nilore, 45650, Pakistan

<sup>e</sup> Tsinghua University, School of Materials Science and Engineering, Key Laboratory of Advanced Materials, Beijing, 100084, China

<sup>f</sup> Hydro Aluminium AS, Research and Technology Development, Sunndalsøra, 6600, Norway

\* corresponding author: mahmood.khan@ntnu.no

**ABSTRACT.** Friction stir welding is a solid-state welding process used extensively for aluminium alloys. EN AW-1100 alloy is mostly used for its exceptional corrosion resistance, high ductility, high thermal and electrical conductivities, and cost-effectiveness. This study is focused on the optimisation of friction stir welding parameters to achieve enhanced mechanical properties of 5 mm thick EN AW-1100 alloy plates welded with a single pass, using Taguchi L9 orthogonal array and ANOVA analysis. Experimental results revealed that maximum tensile strength of 79 MPa and percentage elongation of 38.87 % were achieved. The maximum Vickers hardness achieved in the stir zone was 34.15. These results were used for optimisation using Minitab and it was determined that 2000 RPM, 30 mm·min<sup>-1</sup> traverse speed and square probe profile came out to be the best parameters for maximum tensile strength. 4000 RPM, 30 mm·min<sup>-1</sup> traverse speed and square probe geometry were the best parameters for maximum hardness in the stir zone. ANOVA analysis showed that the most significant parameter for tensile strength was traverse speed. None of the considered parameters were influencing the hardness value in the stir zone at a 95 % confidence level.

**KEYWORDS:** Friction stir welding, parametric optimisation, mechanical properties, Taguchi method, ANOVA, aluminium alloys, EN AW-1100 alloy.

### 1. INTRODUCTION

Aluminium alloys are broadly used in different areas [1, 2]. These include marine, railways, nuclear, aerospace, and automobile industries [3]. Aluminium-1100 alloy (EN AW-1100) is used in electrical bus bars, radiator components, heat exchangers, and fuel tanks [4]. It is also used in cowlings and oil tanks of aircrafts, fin blades, fin stocks, flue linings, and sheet metal works [5, 6]. Chemical processing equipment, automotive body panels, and building dampers also involve EN AW-1100 parts [7, 8]. Conventional welding of aluminium alloys is problematic due to the solidification cracking [9], porosity, embrittlement [10], shrinkage [11], higher solubility of hydrogen, and the formation of oxide layers [12]. The welding institute (TWI) brought up a new joining technique for aluminium alloys called Friction Stir Welding (FSW) in 1991 [13]. FSW involves a specialised non-consumable

tool [14]. The tool mixes while plastically deforming the material to form the joint [15]. The detrimental effects of the heat-affected zone (HAZ) are reduced in FSW [3]. This is because the heat input and peak temperatures are considerably lower than in the conventional welding techniques [16]. The process is repeatable [17], environment friendly [18], and produces minimum waste [19]. It is a solid-state process [20], can be used in joining of various structural materials [21], and has a possibility of being extended to dissimilar metal welding [22]. Figure 1 shows the schematics of the FSW process and subsequent approach.

The weld properties are quite sensitive to the parameters at which welding is executed. Welding parameters affect the mechanical properties, energy consumption, quality, defect formation, and morphology of the weld [23]. The parameters significantly influencing the

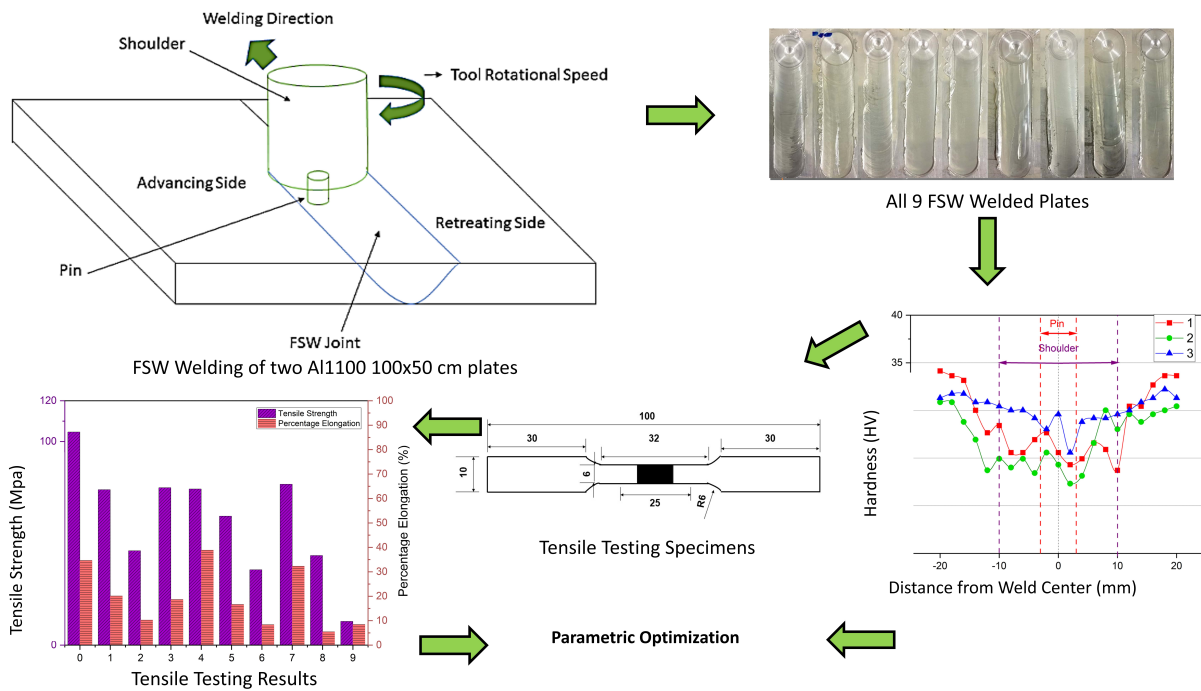


FIGURE 1. Process schematics of FSW welding and successive experimental approach.

microstructure and mechanical properties include rotational speed, traverse speed, and tool geometry [24]. Due to improper selection of parameters, numerous defects arise in the weldment including kissing bonds, tunnelling, cracks, voids, flash, and lack of penetration [25]. This study addresses the optimisation of welding parameters on FSW of EN AW-1100 alloy using Taguchi design of experiments and other aiding methods, namely Matrix Plots, S/N ratio method and ANOVA analysis with the help of different experimental techniques. Taguchi method is being employed in which several factors can be optimised at the same time and quantitative data can be acquired with lesser experimental effort as compared to other methods [26]. ANOVA is more useful in the simultaneous comparison of numerous predictor variables and their levels, which is preferable for the comparison of three or more variables, and is faster and easier to use [27].

Several attempts have been made on studying the effects of different parameters on the microstructure and mechanical properties of Aluminium alloys. Pandey et al. performed a study on defect formation during FSW on EN AW-1100 alloy by varying traverse speed and rotational speed. The high rotational speed with lower traverse speed resulted in the formation of voids due to excessive heat generation whereas craters and micro tunnels were found for low traverse and low rotational speed [28]. Dialmi et al. [29] studied defect formation in friction stir welding and found abnormal stirring and insufficient and excessive heat input to be the main causes of defect formation. Wormholes and tunnelling defects occur due to poor heat input

and improper stirring whereas flashing occurs due to higher heat generation (higher rotational speed and low traverse speed). Voids and cavity-type defects are formed when both the rotational speed and the traverse speed are high.

V. John et al. [30] used Taguchi Method and performed parametric analysis using traverse speed, rotational speed, and shoulder diameter for several tool materials on EN AW-6082 alloy using ANOVA to conclude that the rotational speed was of prime importance. Vahid et al. [31] studied the effect of probe shape and shoulder surface for EN AW-6061 alloy using six different tools. The results showed that the conical shoulder with a threaded square probe gave the highest tensile strength. Suresha et al. [32] utilised the Taguchi method and ANOVA analysis to perform the study for different probe profiles. Welding parameters including RPM, heel plunge depth, and traverse speed were used and it was determined that RPM had a major effect on the tensile strength. Balasubramanian et al. [33] performed a study on the influence of the probe profile with rotational speed, shoulder diameter, and traverse speed on FSW of EN AW-2219 and EN AW-6061 alloys to conclude that the square tool produces mechanically and metallurgically defect-free welds.

The influence of the probe profile (of WC bases tools), traverse speed, and rotational speed was investigated by Tamadon et al. [34] Tensile strength and weld morphology were studied. Different structural defects were found and results emphasised the need for parametric optimisation. Optimisation of traverse speed,

a) Chemical Composition of EN AW-1100 alloy						
Element	Si	Fe	Cu	Mn	Mg	Cr
Wt%	0.84	0.32	0.002	0.002	0.002	0.02
Element	Ni	Zn	Ti	Pb	S/N	Al
Wt%	0.012	0.017	0.08	0.03	0.005	Balance
b) Chemical Composition of D2 for FSW tool						
Element	C	Si	Mn	P	S	Cr
Wt%	2.23	0.5	0.34	0.02	0.004	11.07
Element	Mo	Ni	Al	W	V	Fe
Wt%	0.11	0.2	0.12	0.11	0.14	Balance
c) Selected parameters for FSW of EN AW-1100 alloy						
Parameters		Level 1	Level 2	Level 3		
Rotational Speed [RPM]		2000	3000	4000		
Traverse Speed [mm·min <sup>-1</sup> ]		30	50	70		
Probe Geometry		Cylindrical (Cy)	Tapered (T)	Square (S)		

TABLE 1. Chemical Composition of EN AW-1100 alloy and D-2 steel for FSW tool as determined by OES and FSW parameters.

tilt angle, and rotational speed for percentage elongation and hardness for dissimilar friction stir welding between 5 mm plates of EN AW-5083 and EN AW-6061 alloys was executed by Prasad et al. [35] It was concluded that the major contributing parameter to percentage elongation and hardness at the stir zone was traverse speed. Nakowong et al. [36] performed an optimisation study on FSW butt-welded semi-solid EN AW-5083 alloy using the Taguchi method and ANOVA analysis for tensile strength and hardness. The considered parameters included traverse speed, rotational speed, and tool probe profile and it was concluded that the traverse speed was the most influential parameter for tensile strength whereas none of the parameters was significant for hardness.

Understanding the importance of the effects of welding parameters and the need for their optimisation to minimise defects and to maximise the hardness (at the stir zone) and tensile strength of the weld joints at somewhat higher rotational speeds, utilising the above studies and their commendable research approach, authors have hereby attempted to present an insight on the optimisation of rotational speed, traverse speed, and tool probe profile for a single pass FSW of EN AW-1100 alloy plates in butt-weld configuration using Taguchi method for the design of the experiment (DOE). Radiographic test, Tensile testing, and Vickers hardness were also used for the analysis. Higher rotational speeds were used to reduce the manufacturing time and Matrix Plots, S/N ratio method and ANOVA analysis were then applied to determine the effect of parameters, their percentage contribution, significant parameters, and the optimal level of each parameter for desired maximum hardness (at stir zone) and tensile strength using Minitab 19 software. The results are discussed in light of relevant studies and presented with ease of understanding and prospects of FSW for the research community.

## 2. MATERIALS AND METHODS

### 2.1. MATERIALS

A 5 mm thick sheet of EN AW-1100 alloy was used for FSW. The composition of EN AW-1100 alloy obtained from Spark optical emission spectroscopy (OES) is shown in Table 1a. The samples were cut from the sheet with dimensions of 100 × 50 × 5 mm. The two plates were placed adjacent to each other with no gap in between. SS 304 of 3 mm thickness was chosen as the backing plate due to its lower thermal diffusivity. D-2 steel was used for the manufacturing of the tools. The composition of D-2 steel determined by Spark OES is shown in Table 1b.

### 2.2. TOOL DESIGN

Tools were designed having the same shoulder diameter of 20 mm and probe length of 4 mm. The diameter of the cylindrical probe was 6 mm and the larger diameter of the taper probe was 6 mm [37]. The tool design is shown in Figure 2a whereas the tools used are shown in Figure 2b.

### 2.3. PROCESSING SETUP

A milling machine was used for the FSW process. The tool was held by the collet. Plates were clamped in position by using the stair clamps. The welding was performed in a single pass. Figure 2c shows the experimental setup with a zoom view in Figure 2d.

The clamps were tightened such that there was no gap between the plates. Before the welding process, the tool was traversed manually along the centreline of plates to ensure that the tool remained in the centre throughout the process. The dwell time was 20 seconds, same for all experiments.

### 2.4. TECHNIQUES USED FOR ANALYSIS

#### 2.4.1. RADIOGRAPHIC TESTING

A radiographic test was performed using Andrex 300 kV X-ray machine (70 kV tube voltage with an ex-

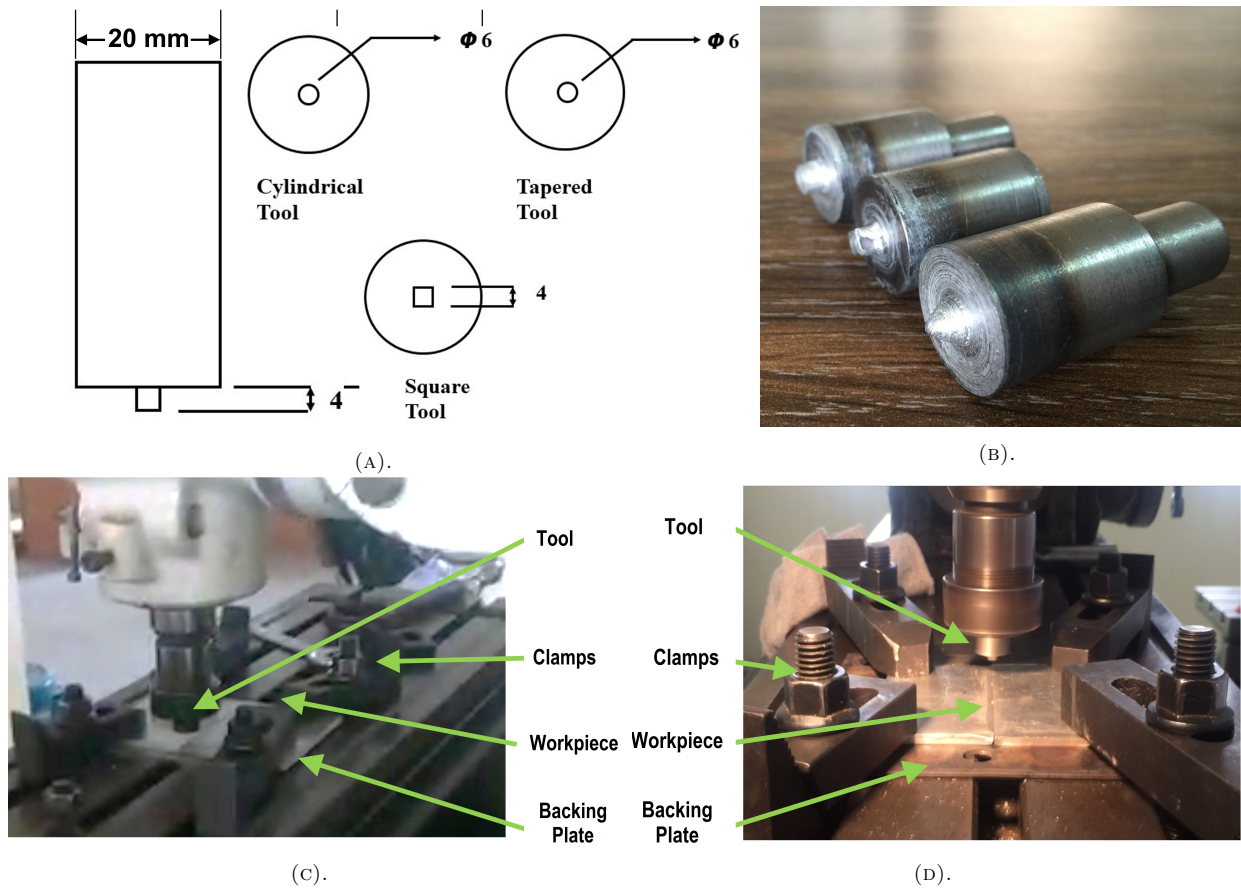


FIGURE 2. Pictures of; (A) the designed tool for FSW, (B) the used tools, (C) the milling machine setup and (D) a close-up view of the experimental setup from a different angle.

posure of 4 mA·min). X-rays were passed through the welds and results were observed on the radiographic film.

#### 2.4.2. HARDNESS ANALYSIS

Vickers hardness analysis was performed according to ASTM E384 and ASTM E92 standards. The load of 2 kg was used, and indents were formed with a spacing of 1 mm up to 10 mm on both sides from the centre (0 position) to develop a hardness profile as shown in macro-etched embossed in the hardness profile Figure 3. The indent's dimensions were measured and the hardness (HV) was calculated based on the known force. The dwell time was 15 seconds as per standard.

#### 2.4.3. TENSILE TESTING

Tensile strength was measured and ASTM E08/E8M was used for the subsize specimen (Total length 100 mm, gauge length 25 mm and width of small section 6 mm) using an Electromechanical Universal Testing Machine. The strain rate of the test was  $5 \text{ mm} \cdot \text{min}^{-1}$ , and the “load vs displacement” curves were obtained. From these curves, “stress vs strain” curves were obtained. From the maximum load, tensile strength was calculated as the area was previously known from the dimensions of the specimen. Percentage elongation was calculated from the original length of the specimen and displacement produced during

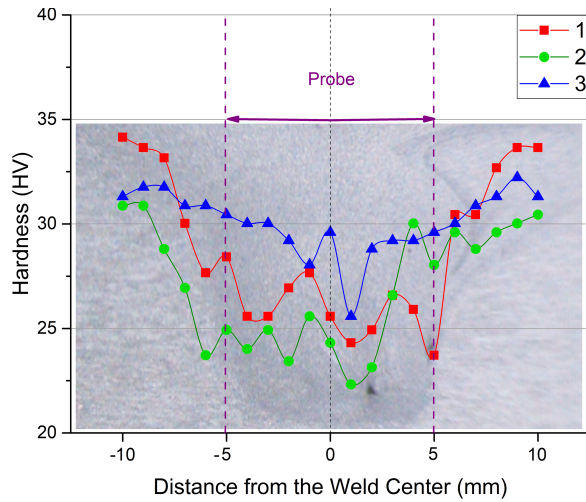
the testing. The tensile strength of the base material was measured by the same machine. Joint efficiencies were calculated as the ratio of tensile strength of the weld sample to that of the base material.

#### 2.4.4. DESIGN OF EXPERIMENTS USING THE TAGUCHI METHOD

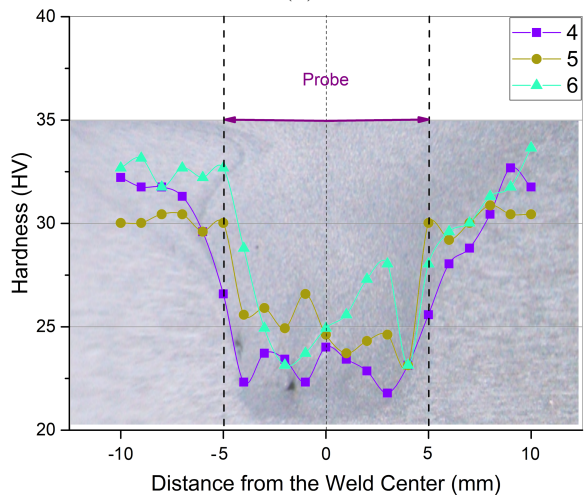
Taguchi method developed by Japanese scientist Genichi Taguchi utilises statistical techniques and quality loss function for analysing the effect of parameters and their optimisation [38]. The Taguchi method can be summarised in the following steps [39]:

- (1.) Selection of parameters to be optimised.
- (2.) Selection of their number of levels.
- (3.) Choice of the orthogonal array.
- (4.) Conducting the experiments.
- (5.) Collection of results through analysis.
- (6.) Statistical analysis for optimisation using experimental results.

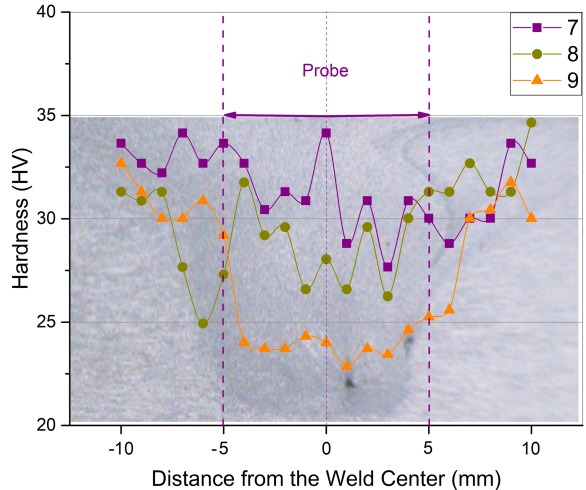
Rotational speed, traverse speed, and probe geometry were selected for the optimisation. Experiments were carried out initially on the plates on different parameters and from their visual examination, the range of parameters was finalised. Higher rotational speeds, 2000, 3000 and 4000 RPM, were chosen to decrease



(A).



(B).



(C).

FIGURE 3. Hardness profile of welds numbers, (A) 1-3 (B) 4-6 (C) 7-9.

the processing time whereas the traverse speeds of  $30, 50$  and  $70 \text{ mm}\cdot\text{min}^{-1}$  and tool tilt angle of  $0^\circ$  was used. Three different probe geometries, cylindrical, tapered, and square were used [37]. Selected parameters/ factors with their levels are shown in Table 1c.

Sample No.	Rotational Speed [RPM]	Traverse Speed [ $\text{mm}\cdot\text{min}^{-1}$ ]	Probe Geometry
1.	2000	30	Cylindrical
2.	2000	50	Tapered
3.	2000	70	Square
4.	3000	30	Tapered
5.	3000	50	Square
6.	3000	70	Cylindrical
7.	4000	30	Square
8.	4000	50	Cylindrical
9.	4000	70	Tapered

TABLE 2. L9 orthogonal array used for experimentation.

For this study L9, orthogonal array was used as shown in Table 2.

## 2.5. PARAMETRIC OPTIMISATION

Matrix plots were generated to understand the behaviour of the independent variables on the two dependent variables (tensile strength and hardness value at the stir zone). Signal-to-noise ratio (S/N ratio) was used for hardness and tensile strength and “main effects plots” for means and S/N ratios were determined to get the best configuration of parameters for maximum hardness and tensile strength. A Higher S/N ratio indicates better weld properties. The S/N ratio is calculated using the following formula [40]:

$$\frac{S}{N} = -10 \log_{10} \frac{1}{n} \sum_{i=1}^n \frac{1}{y_i^2} \quad (1)$$

ANOVA analysis (statistical method) was then used to obtain the percentage contribution of the parameters and to identify the most significant parameter. Minitab 19 was used for these methods.

## 3. RESULTS AND DISCUSSION

### 3.1. RADIOGRAPHIC TESTING

Figure 4a shows the welds along with the result of the radiographic test in Figure 4b. The samples' numbers with the respective parameters are mentioned below the Figure 4b and can be seen in Table 2. The weld comprises  $20 \text{ mm}$  area (same as the shoulder diameter) whereas the length of the welded plates is  $100 \text{ mm}$ . The intensity difference shows the non-homogeneity of the material. The dark lines (indicated by black and red lines) show the lack of material whereas the bright lines show the material accumulation (indicated by yellow arrows) on a radiograph. The black circles correspond to the exit hole (indicated by the orange arrow in the first weld). This hole is produced at the end of the weld as the tool is removed and the whole cavity is left behind [9].

The broad black line shows the presence of a lack of fusion, tunnelling or void type of a linear defect (indicated by black lines). The sharp dark line at the centre indicates the lack of penetration (indicated by

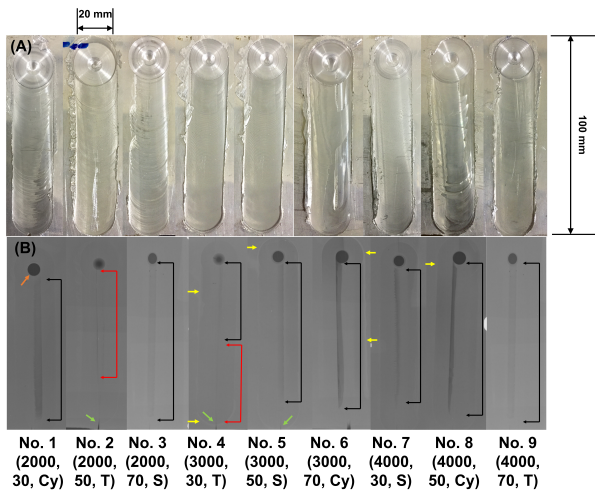


FIGURE 4. Visual appearance of FSW joints (A) and radiographs of all the FSW joints (B).

red lines). The bright line surrounding the welded area (at the tool shoulder boundary indicated by yellow arrows) shows the material accumulation due to flashing as a flat shoulder tool was used [41]. The line originating from the start of the tool in some samples (indicated by green arrows) is due to the drilling and punching during the plunging of the tool. The plunging tool has exerted stress on the base material and displaced it.

The heat generation increases with the increase in rotational speed and decreases with increasing traverse speed. A certain combination of these parameters generates excess heat due to which the material expands and a certain amount of material is lost due to flashing. When the tool moves forward, the material starts to cool down. The material cooling occurs in two possible ways, one from the surface to the atmosphere and the other by conduction in the material. If the cooling by convection is more significant than the other, the surface will be colder than the bulk of the material. The material will contract, but due to the material loss in flashing, a certain linear defect will form [28].

### 3.2. HARDNESS ANALYSIS

Figure 3a shows the Vickers hardness profile for samples 1, 2, and 3, Figure 3b then for 4, 5, and 6 and Figure 3c for 7, 8 and 9. The dashed lines show the probe region and the shoulder region. The zero position is the centreline of the welded plates. A “W” shaped trend is observed in the variation of hardness, i.e. the value decreases in the welding region (shoulder area) with a small increase in the probe region. The hardness in the region outside the shoulder increases and appears to attain a somewhat constant value.

The reason is that the welding area (Figure 5a) consists of different zones as shown in Figure 5, prevailing to the probe rotation thus having different microstructures and properties including the stir zone (Figure 5b), Thermo-mechanically affected zone (TMAZ, Figure 5d), Heat affected zone (HAZ) and unaffected

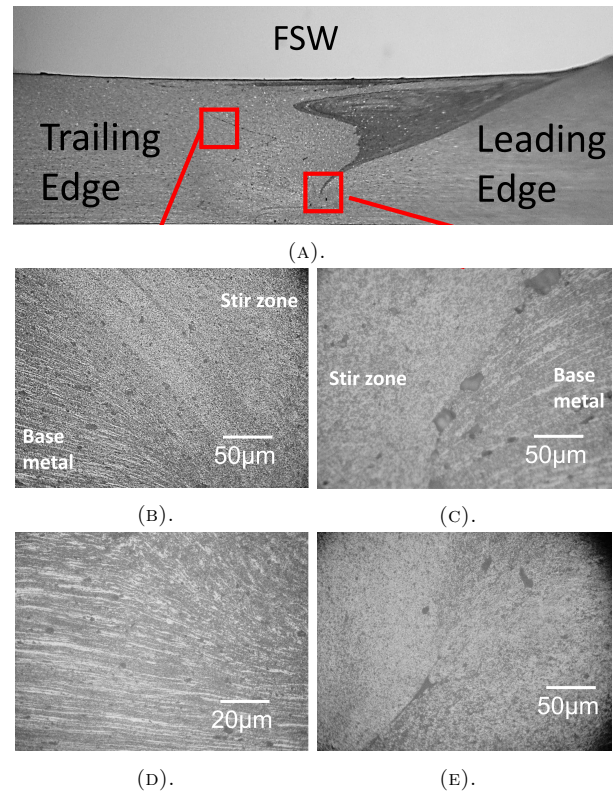


FIGURE 5. Microstructures of FSW sample with distinct regions; (A) macro-etched cross-section of FSW EN AW-1100 alloy plate, (B) trailing edge of the stir zone (right) and base metal (left), (C) leading edge microstructure indicating stir zone (left) and base metal (right), (D) thermo-mechanically affected zone microstructure and (E) FSW defect as revealed in radiographic testing.

zone (base metal, Figure 5c). The stir zone in the centre is a highly plastically deformed area, formed due to excessive stresses exerted by the tool [42]. It has fine equi-axed grains which increase the hardness as a decrease in grain size results in an increase in hardness value and vice versa, as related by the Hall-Petch Equation [43, 44]. The welded area (within the shoulder) shows a drop in the hardness value due to the heat produced during welding and recrystallisation mechanisms. In the HAZ, heat and higher temperatures cause the coarsening of the grains and hardness drops. The hardness value then increases and approaches a constant value in the unaffected base metal. As shown in Figure 3, sample number 3, 5, and 7 show the highest values in the probe region, these are welded with square probe. The square probe exerts higher stresses due to flat faces and deforms the grains to a higher extent, which increases the hardness values.

Das et al. [45] performed a study on FSW of EN AW-2014 alloy using different probes and concluded that the square geometry gives increased hardness due to its pulsating stirring, increased plastic deformation, better recrystallisation and excellent metal interlocking during welding. The “W” shaped hardness dis-

tribution is consistent with the study performed by Jimmy et al. [46] to understand the effect of shoulder geometry on properties of EN AW-1100 alloy by FSW. The hardness values and trends showed the same behaviour: a decrease in the welding area with small increase in hardness in the probe region of the stir zone (Figure 5e). Yupeng Li et al. [47] concluded a study on the effect of rotational and traverse speeds on the microstructure and mechanical properties of EN AW-6082-T6 alloy using a bobbin tool. The hardness distribution was also found out to be “W” shaped.

### 3.3. TENSILE TESTING

Figures 6a and 6b shows the tensile test specimens before and after the testing, respectively. Figure 6c shows the stress-strain curves and Figure 6d shows the comparison of tensile strength and percentage elongation of all samples.

Table 3 shows the mechanical properties of the base metal (Sample 0) along with the results of the tensile testing of all specimens. The testing of the base metal is performed using the same standard and machine as the rest of the samples for comparison.

The results showed that sample 4 and sample 7 exhibited the best results in terms of the percentage elongation and samples 1, 3, 4, and 7 showed the best tensile strength. The samples welded by the tapered tool exhibited the lowest tensile strength whereas the square tool gave better results and will be discussed in section 3.5.

The joint efficiency of most of the samples is around 70–80%. The reason for this behaviour is due to the presence of different zones in the welded material. The Stir zone consists of fine grains (as shown in Figure 5b) due to the dynamic recrystallisation and an “onion-ring” structure is formed, which improves the properties, whereas HAZ results in the degradation of strength [42]. The excessive heat involved in the process broadens the HAZ and the precipitates which strengthen the joint get dissolved in the HAZ/TMAZ and this region softens; leading to the decrease in strength of the weldment as compared to the strength of base metal [48].

### 3.4. PARAMETRIC OPTIMISATION FOR ENHANCED HARDNESS IN THE STIR ZONE (0 POSITIONS)

For maximum hardness (in the stir zone), the results of matrix plots, S/N ratios, main effect plots and ANOVA analysis are discussed in this section.

#### 3.4.1. MATRIX PLOTS

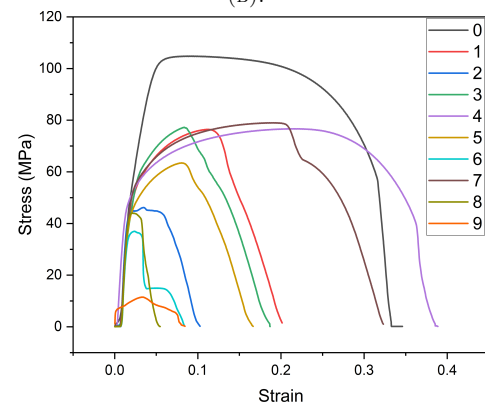
For hardness, the matrix plots are shown in Figure 7. The increase in RPM results in an increase in the hardness of the stir zone. The increase in the traverse speed results in a slight decrease in the hardness whereas the hardness reaches highest values for the square tool.



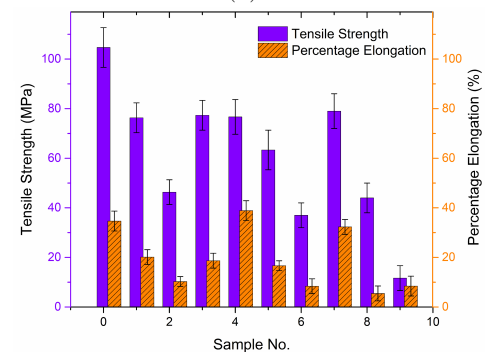
(A).



(B).



(C).



(D).

FIGURE 6. Pictures of; (A) tensile test specimens before testing, (B) after testing, (C) Stress-Strain curves and (D) comparison of tensile strength and % Elongation of all the samples.

The second row shows the effect of traverse speed and probe profile on RPM. As these all are independent variables, so they do not affect each other and show a straight line. Similarly, the third row shows

Sample No.	Rotational Speed [RPM]	Traverse Speed [mm·min <sup>-1</sup> ]	Probe Geometry	Tensile Strength [MPa]	Joint Efficiency [%]	Percentage Elongation [%]
0. (Base Metal)	-	-	-	104.67	-	34.6
1.	2000	30	Cylindrical	76.33±7	72.93	20.14±3
2.	2000	50	Tapered	46.33±5	44.27	10.27±2
3.	2000	70	Square	77.33±6	73.88	18.69±3
4.	3000	30	Tapered	76.67±7	73.25	38.87±4
5.	3000	50	Square	63.33±8	60.51	16.65±2
6.	3000	70	Cylindrical	37.00±5	35.35	8.38±3
7.	4000	30	Square	79.00±8	75.48	32.31±4
8.	4000	50	Cylindrical	44.00±6	42.04	5.47±3
9.	4000	70	Tapered	11.67±5	11.15	8.45±4

TABLE 3. Tensile testing results of the samples.

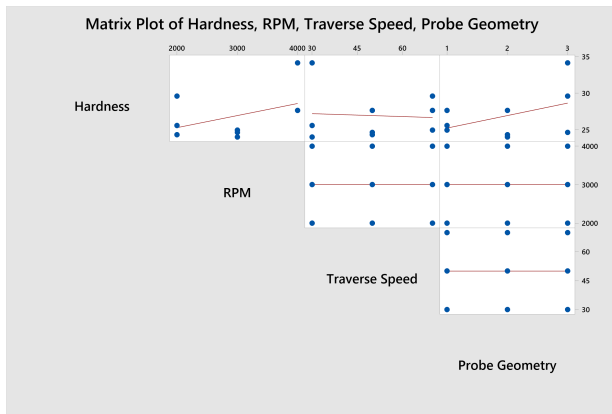


FIGURE 7. Matrix Plots for Hardness.

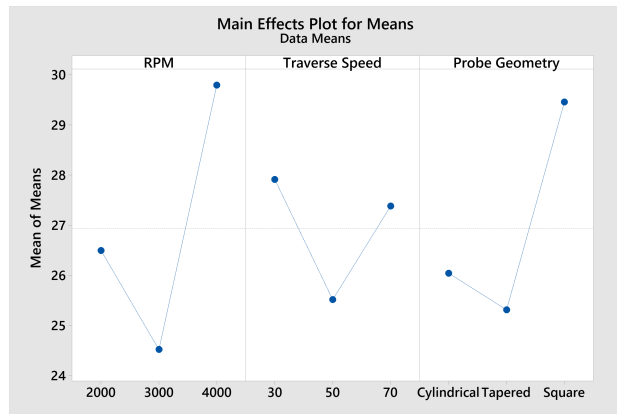


FIGURE 8. Main effect plot for means.

that there is no effect of the probe profile on the traverse speed.

### 3.4.2. SIGNAL-TO-NOISE RATIO (S/N RATIO)

Table 4 shows the S/N ratio values for the hardness. The available options are “Smaller the better”, “Nominal the better” and “Larger the better”. “Larger the better” was selected for the optimisation as higher hardness in the nugget zone is the desired outcome.

Table 5 shows the response table for means for Hardness. It is evident that level 3 of RPM has a maximum response of 29.8 and level 1 of traverse speed has a maximum response of 27.91. Level 3 of probe geometry gave the maximum response of 29.46. It also shows the response table for the S/N ratio for Hardness. It is evident that level 3 of RPM has a maximum response of 29.44 and level 1 of traverse speed has a maximum response of 28.81. Level 3 of the probe geometry gave the maximum response of 29.31.

Figure 8 shows the “main effect plots” for means and Figure 9 shows the “main effect plots” for S/N ratios.

Figures 7, 8 and 9 shows that the maximum hardness is reached for 4000 RPM, 30 mm·min<sup>-1</sup> traverse speed, and square probe profile, hence these are the best parameters. The variation of mechanical prop-

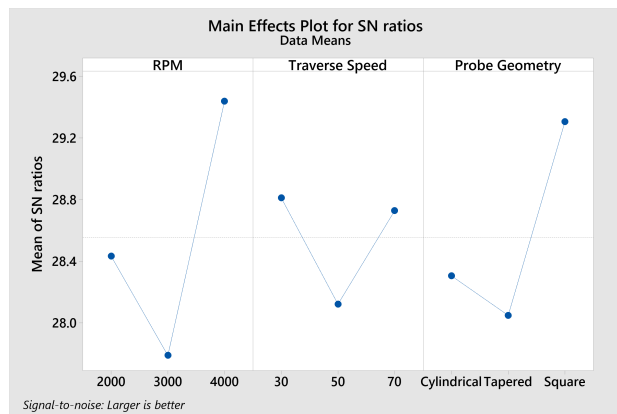


FIGURE 9. Main effect plot for S/N ratios.

erties during FSW for different ranges of rotational and traverse speeds is different, depending on their combined effect. The rotational speed, traverse speed, and tool probe profile controls the grain refinement and the peak temperatures during welding [49].

The rotational speed deforms the material and produces frictional heat. The larger the rotational speed, the higher will be the recrystallisation and deformation and hence the grain refinement in the nugget zone [50]. Also, a higher rotational speed and lower traverse speed increase the peak temperatures to coarsen the

Sample No.	Rotational Speed [RPM]	Traverse Speed [mm·min <sup>-1</sup> ]	Probe Geometry	Vickers Hardness	S/N Ratio
1.	2000	30	Cylindrical	25.58±2	28.15
2.	2000	50	Tapered	24.31±2	27.71
3.	2000	70	Square	29.60±3	29.42
4.	3000	30	Tapered	24.01±2	27.60
5.	3000	50	Square	24.62±3	27.82
6.	3000	70	Cylindrical	24.93±3	27.93
7.	4000	30	Square	34.15±3	30.66
8.	4000	50	Cylindrical	27.62±2	28.82
9.	4000	70	Tapered	27.62±3	28.82

TABLE 4. S/N ratio results.

Response Table for Means			
	Rotational Speed [RPM]	Traverse Speed [mm·min <sup>-1</sup> ]	Probe Geometry
Level			
1	26.5	27.91	26.04
2	24.52	25.52	25.31
3	29.8	27.39	29.46
Delta	5.28	2.4	4.14
Rank	1	3	2

Response Table for S/N Ratio			
	Rotational Speed [RPM]	Traverse Speed [mm·min <sup>-1</sup> ]	Probe Geometry
Level			
1	28.43	28.81	28.31
2	27.79	28.12	28.05
3	29.44	28.73	29.31
Delta	1.65	0.69	1.26
Rank	1	3	2

TABLE 5. Response Table for Hardness.

grains. Hence their combined effect determines which effect will dominate the grain refinement. Hardness is the highest for the square tool as the tool having flat faces produces a larger deformation, constant dynamic recrystallisation, and better mixing resulting in finer grains [51]. The tapered tool gives the lowest hardness value. Gupta et al. [52] performed a study on the tool probe profile on FSW of EN AW-1120 and concluded that the tapered tool gave the lowest hardness and tensile strength.

### 3.4.3. ANOVA ANALYSIS

The results are shown in Table 6. The probe geometry showed the largest contribution of 20.12%, followed by the rotational speed (18.86%) and probe geometry. 60.53% contribution is from error which indicates that some significant parameters affecting the hardness are missing (not considered). All the parameters have a p-value greater than 0.05, which shows that none of the considered parameters affected hardness at a 95% confidence level.

Source	Contribution	F-value	P-value
Rotational Speed	18.86%	1.56	0.267
Traverse Speed	0.48%	0.04	0.850
Probe Geometry	20.12%	1.66	0.254
Error	60.53%	-	-
Total	100.00%	-	-

TABLE 6. ANOVA analysis results.

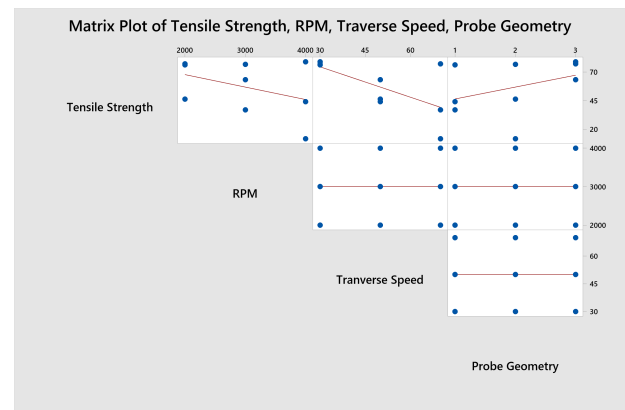


FIGURE 10. Matrix Plot for tensile strength.

## 3.5. PARAMETRIC OPTIMISATION FOR ENHANCED TENSILE STRENGTH

To maximise tensile strength as an output (dependent) variable, the results of matrix plots, S/N ratios, main effect plots and ANOVA analysis are discussed in this section.

### 3.5.1. MATRIX PLOTS

Figure 10 shows the matrix plots for the tensile strength. The first rows show the effects of the parameters on tensile strength. The increase in RPM results in a decrease in tensile strength and the same can be said for the traverse speed. The change in geometry of the probe shows an increase in the tensile strength. The other graphs indicate that the independent variables do not affect each other.

Sample No.	Rotational Speed [RPM]	Traverse Speed [mm·min <sup>-1</sup> ]	Probe Geometry	Vickers Hardness	S/N Ratio
1.	2000	30	Cylindrical	76.33±7	37.65
2.	2000	50	Tapered	46.33±5	33.32
3.	2000	70	Square	77.33±6	37.77
4.	3000	30	Tapered	76.67±7	37.69
5.	3000	50	Square	63.33±8	36.03
6.	3000	70	Cylindrical	37.00±5	31.36
7.	4000	30	Square	79.00±8	37.95
8.	4000	50	Cylindrical	44.00±6	32.87
9.	4000	70	Tapered	11.67±5	21.34

TABLE 7. S/N ratio results.

Response Table for Means			
Level	Rotational Speed [RPM]	Traverse Speed [mm·min <sup>-1</sup> ]	Probe Geometry
1	66.66	77.33	52.44
2	59	51.22	44.89
3	44.89	42.00	73.22
Delta	21.77	35.33	28.33
Rank	3	1	2

Response Table for S/N Ratio			
Level	Rotational Speed [RPM]	Traverse Speed [mm·min <sup>-1</sup> ]	Probe Geometry
1	36.25	37.77	33.96
2	35.03	34.07	30.78
3	30.72	30.16	37.25
Delta	5.53	7.61	6.47
Rank	3	1	2

TABLE 8. Response Table for Hardness.

### 3.5.2. S/N RATIO

The S/N ratio represents the ratio of means to the standard deviation. Three categories, namely “Smaller the better”, “Nominal the better” and “Larger the better” are used for the analysis [53]. For higher tensile strength as the desired outcome, “Larger the better” was chosen for the optimisation. Table 7 shows the calculated S/N ratios.

Table 8 shows the response table for means for Tensile Strength. It is evident that level 1 of RPM has a maximum response of 66.66 and level 1 of traverse speed has a maximum response of 77.33. Level 3 of probe geometry gave the maximum response of 73.22.

It also shows the response table for the S/N ratio for Tensile Strength. Level 1 of RPM has a maximum response of 36.25 and level 1 of traverse speed has a maximum response of 37.77. Level 3 of probe geometry gave the maximum response of 37.25.

Figures 11 and 12 shows the “main effect plots” for means and the “main effect plots” for S/N ratios, respectively. These plots show the results of the parameters for the desired output, which is higher tensile

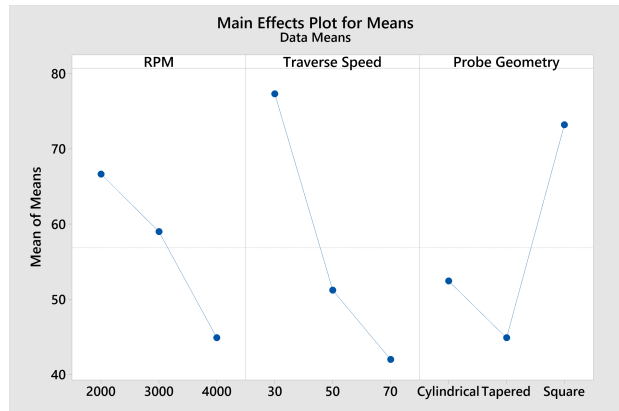


FIGURE 11. Main effect plot for means.

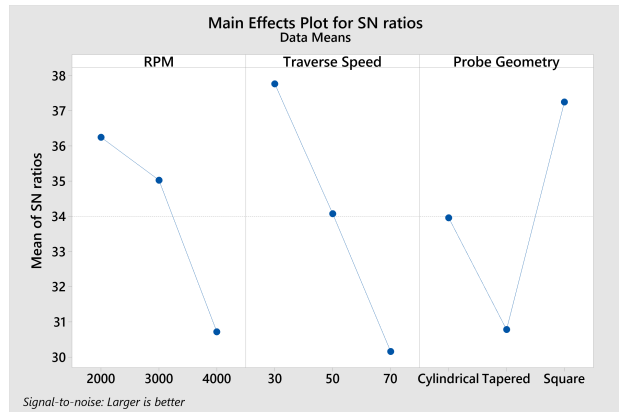


FIGURE 12. Main effect plot for S/N.

strength in this case.

It can be seen from Figures 10, 11, and 12, that an increase in the rotational speed decreases the tensile strength. The reason is that the rotational speed is to be chosen carefully for the best results. On the one hand, a lower rotational speed produces less heat, which results in inadequate softening, leading to insufficient stirring and strength. On the other hand, larger rotational speeds will produce more heat; resulting in the release of stirred material to the upper surface and producing flash, voids, cavity, and tunnel-type defects [54]. Furthermore, the increase in rotational

speed results in larger heat generation, which broadens the HAZ, leading to a lower tensile strength [55]. Hence, the trend of the rotational speed depends on the range that has been chosen and 2000 RPM gives the maximum tensile strength.

Similarly, a particular traverse speed is required to maximise tensile strength. A larger traverse speed will result in rapid cooling and insufficient time for stirring and heat generation. However, a lower traverse speed will produce greater heat and the material will experience a broadening of the HAZ, thereby decreasing the tensile strength [56]. Similarly, in this case, the lowest traverse speed of  $30 \text{ mm}\cdot\text{min}^{-1}$  gave the highest tensile strength.

The probe geometry also affects the strength of the weldment because the probe primarily deforms the material plastically and then mixes it. The shape that will execute both targets will give the best strength. In our case, the square tool gives the best strength followed by cylindrical and then tapered one, as anticipated. The probe geometry having flat faces results in larger effectiveness due to the associated eccentricity [54]. It helps in better mixing as the material passes around the probe due to this property. Also, the probe with flat faces produces pulsating stirring action, resulting in better homogeneity and finer grains, thereby giving better strength. This feature is less effective for cylindrical and tapered tools. Hence, the best parameters for maximum tensile strength are a rotational speed of 2000 RPM, traverse speed of  $30 \text{ mm}\cdot\text{min}^{-1}$  and square tool probe geometry.

### 3.5.3. ANOVA ANALYSIS

The results are shown in Table 9. The traverse speed showed the largest contribution of 42.22%, followed by the rotational speed (16.03%) and probe geometry. The factor having a p-value lesser than 0.05 (at 95% confidence level), i.e. the traverse speed is the most significant parameter affecting the tensile strength.

Source	Contribution	F-value	P-value
Rotational Speed	16.03%	2.95	0.146
Traverse Speed	42.22%	7.78	0.039
Probe Geometry	14.6 %	2.69	0.162
Error	27.15%	-	-
Total	100.00%	-	-

TABLE 9. ANOVA analysis results.

## 4. CONCLUSIONS

In this study, an experimental investigation of a single pass friction stir welding on 5 mm thick EN AW-1100 alloy plates using D2 steel tools and parametric optimisation of rotational speed (RPM), traverse speed ( $\text{mm}\cdot\text{min}^{-1}$ ), and probe geometry in order to achieve

maximum hardness (in stir zone) and tensile strength was performed. The following conclusions were made:

- (1.) Hardness analysis showed that the hardness value decreased in the welding zone, owing to the presence of FSW defect, as revealed by the radiographic testing. Hardness increased slightly in the stir zone and approached a constant value in the base metal. A joint efficiency value in the range of 70-80% was obtained for most of the joints produced.
- (2.) FSW processing parameters; 4000 RPM,  $30 \text{ mm}\cdot\text{min}^{-1}$  traverse speed, and a square probe geometry were the optimised configuration for maximum hardness at the weld zone. For maximum tensile strength, S/N ratio method showed that 2000 RPM,  $30 \text{ mm}\cdot\text{min}^{-1}$  traverse speed, and a square probe geometry were the optimised configuration of parameters.
- (3.) It was concluded that an increase in RPM and traverse speed results in a decrease in tensile strength. The square tool gave the highest tensile strength and hardness followed by the cylindrical tool. Tapered tool gave the lowest tensile strength and hardness due to minimal stirring compared to the other two probe geometries.
- (4.) ANOVA analysis showed that the traverse speed was the most significant parameter for tensile strength (at 95% confidence level). For hardness (in the stir zone), none of the considered parameters were significant (at 95% confidence level).

## REFERENCES

- [1] M. Khan, R. Ud-Din, W. H. Syed, et al. Spark plasma sintering of boron carbide reinforced aluminum alloy (Al6061) matrix composites. In *2019 16th International Bhurban Conference on Applied Sciences and Technology (IBCAST)*, pp. 35–41. 2019. <https://doi.org/10.1109/IBCAST.2019.8667164>
- [2] M. Khan, M. Zulfaqar, F. Ali, T. Subhani. Microstructural and mechanical characterization of hybrid aluminum matrix composite containing boron carbide and Al-Cu-Fe quasicrystals. *Metals and Materials International* **23**(4):813–822, 2017. <https://doi.org/10.1007/s12540-017-6619-7>
- [3] M. Khan, W. H. Syed, S. Akhtar, R. E. Aune. Friction stir processing (FSP) of multiwall carbon nanotubes and boron carbide reinforced aluminum alloy (Al 5083) composites. In Y. Hovanski, R. Mishra, Y. Sato, et al. (eds.), *Friction Stir Welding and Processing X*, pp. 217–232. Springer International Publishing, Cham, 2019. [https://doi.org/10.1007/978-3-030-05752-7\\_21](https://doi.org/10.1007/978-3-030-05752-7_21)
- [4] C. Ng, S. Yahaya, A. Majid. Reviews on aluminum alloy series and its applications. *Academia Journal of Scientific Research* **5**(12):708–716, 2017. <https://doi.org/10.15413/ajsr.2017.0724>
- [5] S. M. Najm, I. Paniti, T. Trzepieciński, et al. Parametric effects of single point incremental forming on hardness of AA1100 aluminium alloy sheets. *Materials* **14**(23):7263, 2021. <https://doi.org/10.3390/ma14237263>

- [6] M. Khan, R. Ud-Din, A. Wadood, et al. Spark plasma sintering of graphene nanoplatelets reinforced aluminium 6061 alloy composites. In A. Tomsett (ed.), *Light Metals 2020*, pp. 301–311. Springer International Publishing, Cham, 2020. [https://doi.org/10.1007/978-3-030-36408-3\\_44](https://doi.org/10.1007/978-3-030-36408-3_44)
- [7] M. Khan, R. Ud-Din, A. Wadood, et al. Physical and mechanical properties of graphene nanoplatelet-reinforced Al6061-T6 composites processed by spark plasma sintering. *JOM* **72**(6):2295–2304, 2018. <https://doi.org/10.1007/s11837-020-04139-y>
- [8] M. Khan, M. Shahzad, M. A. Basit, et al. A comparative study of carbon nanotubes and graphene nanoplatelets on structure-property relationship of aluminium matrix composites synthesized by spark plasma sintering. In T. S. Srivatsan, P. K. Rohatgi, S. Hunyadi Murph (eds.), *Metal-Matrix Composites*, pp. 21–40. Springer International Publishing, Cham, 2022. [https://doi.org/10.1007/978-3-030-92567-3\\_2](https://doi.org/10.1007/978-3-030-92567-3_2)
- [9] M. Khan, R. ud Din, M. A. Basit, et al. Effects of graphene nanoplatelets and boron carbide on microstructure and mechanical behaviour of aluminium alloy (Al6061) after friction stir welding. *Advances in Materials and Processing Technologies* **8**(3):3148–3164, 2022. <https://doi.org/10.1080/2374068X.2021.1945303>
- [10] G. İpekoğlu, G. Çam. Formation of weld defects in cold metal transfer arc welded 7075-T6 plates and its effect on joint performance. *IOP Conference Series: Materials Science and Engineering* **629**(1):012–007, 2019. <https://doi.org/10.1088/1757-899X/629/1/012007>
- [11] G. Çam, M. Koçak. Microstructural and mechanical characterization of electron beam welded Al-alloy 7020. *Journal of Materials Science* **42**(17):7154–7161, 2007. <https://doi.org/10.1007/s10853-007-1604-z>
- [12] G. Çam, V. Ventzke, J. F. Dos Santos, et al. Characterisation of electron beam welded aluminium alloys. *Science and Technology of Welding and Joining* **4**(5):317–323, 1999. <https://doi.org/10.1179/136217199101537941>
- [13] W. Thomas. Friction stir butt welding, international patent application No. PCT/GB92, 1991. GB Patent Application No. 9125978.8.
- [14] M. Khan, A. Rehman, T. Aziz, et al. Cold formability of friction stir processed aluminum composites containing carbon nanotubes and boron carbide particles. *Materials Science and Engineering: A* **701**:382–388, 2017. <https://doi.org/10.1016/j.msea.2017.05.121>
- [15] G. Çam, V. Javaheri, A. Heidarzadeh. Advances in FSW and FSSW of dissimilar Al-alloy plates. *Journal of Adhesion Science and Technology* **37**(2):162–194, 2023. <https://doi.org/10.1080/01694243.2022.2028073>
- [16] T. Küçükömeroğlu, S. M. Aktarer, G. Çam. Investigation of mechanical and microstructural properties of friction stir welded dual phase (DP) steel. *IOP Conference Series: Materials Science and Engineering* **629**(1):012–010, 2019. <https://doi.org/10.1088/1757-899X/629/1/012010>
- [17] G. Çam, G. İpekoğlu, H. T. Serindağ. Effects of use of higher strength interlayer and external cooling on properties of friction stir welded AA6061-T6 joints. *Science and Technology of Welding and Joining* **19**(8):715–720, 2014. <https://doi.org/10.1179/1362171814Y.0000000247>
- [18] G. Çam, G. İpekoğlu. Recent developments in joining of aluminum alloys. *The International Journal of Advanced Manufacturing Technology* **91**(5):1851–1866, 2017. <https://doi.org/10.1007/s00170-016-9861-0>
- [19] G. Çam, S. Mistikoglu, M. Pakdil. Microstructural and mechanical characterization of friction stir butt joint welded 63%Cu-37%Zn brass plate. *Welding journal* **88**:225s–232s, 2009.
- [20] G. Çam, H. Serindag, A. Çakan, et al. The effect of weld parameters on friction stir welding of brass plates. *Materialwissenschaft und Werkstofftechnik* **39**(06):394–399, 2008. <https://doi.org/10.1002/mawe.200800314>
- [21] T. Küçükömeroğlu, E. Şentürk, L. Kara, et al. Microstructural and mechanical properties of friction stir welded nickel-aluminum bronze (NAB) alloy. *Journal of Materials Engineering and Performance* **25**(1):320–326, 2016. <https://doi.org/10.1007/s11665-015-1838-x>
- [22] T. Küçükömeroğlu, S. M. Aktarer, G. İpekoğlu, G. Çam. Mechanical properties of friction stir welded St 37 and St 44 steel joints. *Materials Testing* **60**(12):1163–1170, 2018. <https://doi.org/doi:10.3139/120.111266>
- [23] J. Victor Christy, A.-H. Ismail Mourad, M. M. Sherif, B. Shivamurthy. Review of recent trends in friction stir welding process of aluminum alloys and aluminum metal matrix composites. *Transactions of Nonferrous Metals Society of China* **31**(11):3281–3309, 2021. [https://doi.org/10.1016/S1003-6326\(21\)65730-8](https://doi.org/10.1016/S1003-6326(21)65730-8)
- [24] M. MohammadiSefat, H. Ghazanfari, C. Blais. Friction stir welding of 5052-H18 aluminum alloy: Modeling and process parameter optimization. *Journal of Materials Engineering and Performance* **30**(3):1838–1850, 2021. <https://doi.org/10.1007/s11665-021-05499-5>
- [25] V. P. Singh, S. K. Patel, B. Kuriachen, S. Suman. Investigation of general welding defects found during friction-stir welding (FSW) of aluminium and its alloys. In M. S. Shunmugam, M. Kanthababu (eds.), *Advances in Additive Manufacturing and Joining*, pp. 587–595. Springer Singapore, Singapore, 2020. [https://doi.org/10.1007/978-981-32-9433-2\\_51](https://doi.org/10.1007/978-981-32-9433-2_51)
- [26] A. V. U. K. Kandala, D. G. Solomon, J. J. Arulraj. Advantages of Taguchi method compared to response surface methodology for achieving the best surface finish in wire electrical discharge machining (WEDM). *Journal of Mechanical Engineering (JMEchE)* **19**(1):185–199, 2022. <https://doi.org/10.24191/jmeche.v19i1.19696>
- [27] B. K. Das, D. N. Jha, S. K. Sahu, et al. Analysis of variance (ANOVA) and design of experiments. In *Concept Building in Fisheries Data Analysis*, pp. 119–136. Springer Nature Singapore, Singapore, 2023. [https://doi.org/10.1007/978-981-19-4411-6\\_7](https://doi.org/10.1007/978-981-19-4411-6_7)
- [28] A. K. Pandey, V. Narayanan. Investigation of defect formation during friction stir welding of aluminum alloys. *AIP Conference Proceedings* **2273**(1):050030, 2020. <https://doi.org/10.1063/5.0024507>

- [29] N. Dialami, M. Cervera, M. Chiumenti. Defect formation and material flow in friction stir welding. *European Journal of Mechanics - A/Solids* **80**:103912, 2020. <https://doi.org/10.1016/j.euromechsol.2019.103912>
- [30] V. John, R. Pant, S. Aggrawal, P. Agarwal. Parametric analysis and effect of tool on FSW joint of 6082 Al alloy by Taguchi method. *International Journal of Mechanical and Production Engineering Research and Development* **8**(1):105–110, 2018. <https://doi.org/10.24247/ijmperdfeb201812>
- [31] V. Moosabeiki, G. Azimi, M. Ghayoor. Influences of tool pin profile and tool shoulder curvature on the formation of friction stir welding zone in AA6061 aluminium alloy. In *Materials and Manufacturing Technologies XIV*, vol. 445 of *Advanced Materials Research*, pp. 789–794. Trans Tech Publications Ltd, 2012. <https://doi.org/10.4028/www.scientific.net/AMR.445.789>
- [32] C. N. Suresha, B. M. Rajaprakash, S. Upadhyaya. A study of the effect of tool pin profiles on tensile strength of welded joints produced using friction stir welding process. *Materials and Manufacturing Processes* **26**(9):1111–1116, 2011. <https://doi.org/10.1080/10426914.2010.532527>
- [33] K. Elangovan, V. Balasubramanian. Influences of tool pin profile and tool shoulder diameter on the formation of friction stir processing zone in AA6061 aluminium alloy. *Materials & Design* **29**(2):362–373, 2008. <https://doi.org/10.1016/j.matdes.2007.01.030>
- [34] A. Tamadon, A. Baghestani, M. E. Bajgholi. Influence of WC-based pin tool profile on microstructure and mechanical properties of AA1100 FSW welds. *Technologies* **8**(2):34, 2020. <https://doi.org/10.3390/technologies8020034>
- [35] M. Prasad, K. kumar Namala. Process parameters optimization in friction stir welding by ANOVA. *Materials Today: Proceedings* **5**(2, Part 1):4824–4831, 2018. 7th International Conference of Materials Processing and Characterization, March 17-19, 2017. <https://doi.org/10.1016/j.matpr.2017.12.057>
- [36] K. Nakowong, K. Sillapasa. Optimized parameter for butt joint in friction stir welding of semi-solid aluminum alloy 5083 using Taguchi technique. *Journal of Manufacturing and Materials Processing* **5**(3):88, 2021. <https://doi.org/10.3390/jmmp5030088>
- [37] G. Ghangas, S. Singhal. Effect of tool pin profile and dimensions on mechanical properties and microstructure of friction stir welded armor alloy. *Materials Research Express* **5**(6):066555, 2018. <https://doi.org/10.1088/2053-1591/aacdb1>
- [38] Y. Javadi, S. Sadeghi, M. A. Najafabadi. Taguchi optimization and ultrasonic measurement of residual stresses in the friction stir welding. *Materials & Design* **55**:27–34, 2014. <https://doi.org/10.1016/j.matdes.2013.10.021>
- [39] M. Akbari, P. Asadi. Optimization of microstructural and mechanical properties of brass wire produced by friction stir extrusion using Taguchi method. *Proceedings of the Institution of Mechanical Engineers, Part L: Journal of Materials: Design and Applications* **235**(12):2709–2719, 2021. <https://doi.org/10.1177/14644207211032992>
- [40] P. Ross. *Taguchi Techniques for Quality Engineering: Loss Function, Orthogonal Experiments, Parameter and Tolerance Design*. Industrial engineering. McGraw-Hill, 1988.
- [41] M. Khan, A. Rehman, T. Aziz, et al. Effect of inter-cavity spacing in friction stir processed Al 5083 composites containing carbon nanotubes and boron carbide particles. *Journal of Materials Processing Technology* **253**:72–85, 2018. <https://doi.org/10.1016/j.jmatprotec.2017.11.002>
- [42] L. Dumpala, D. Lokanadham. Low cost friction stir welding of aluminium nanocomposite – a review. *Procedia Materials Science* **6**:1761–1769, 2014. 3rd International Conference on Materials Processing and Characterisation (ICMPC 2014). <https://doi.org/10.1016/j.mspro.2014.07.206>
- [43] E. O. Hall. The deformation and ageing of mild steel: III discussion of results. *Proceedings of the Physical Society Section B* **64**(9):747, 1951. <https://doi.org/10.1088/0370-1301/64/9/303>
- [44] N. J. Petch. The cleavage strength of polycrystals. *Journal of the Iron and Steel Institute* **174**:25–28, 1953.
- [45] J. Das, P. S. Robi, M. R. Sankar. Assessment of parameters windows and tool pin profile on mechanical property and microstructural morphology of FSWed AA2014 joints. *SN Applied Sciences* **2**:123, 2019. <https://doi.org/10.1007/s42452-019-1895-0>
- [46] J. Unfried, J. Rodriguez, A. Torres, J. Carrasco. Effects of shoulder geometry of tool on microstructure and mechanical properties of friction stir welded joints of AA1100 aluminum alloy. *Dyna (Medellin, Colombia)* **84**(200):202–208, 2017. <https://doi.org/10.15446/dyna.v84n200.55787>
- [47] Y. Li, D. Sun, W. Gong. Effect of tool rotational speed on the microstructure and mechanical properties of bobbin tool friction stir welded 6082-T6 aluminum alloy. *Metals* **9**(8):894, 2019. <https://doi.org/10.3390/met9080894>
- [48] S. K. K. Jayakumar. Effect of tool pin profile on the mechanical and microstructural properties of dissimilar friction stir welded AA5083-H111 and AA6061-T6 aluminium alloys. *Journal of the Chinese Institute of Engineers* **45**(3):227–236, 2022. <https://doi.org/10.1080/02533839.2022.2034054>
- [49] D. Hao, T. Tra. Effects of friction stir welding parameters on the mechanical properties of AA7075-T6. *Archives of Materials Science and Engineering* **77**:58–64, 2016. <https://doi.org/10.5604/18972764.1225594>
- [50] D. Sethi, U. Acharya, S. Kumar, et al. Effect of tool rotational speed on friction stir welded AA6061-T6 scarf joint configuration. *Advanced Composites and Hybrid Materials* **5**(3):2353–2368, 2022. <https://doi.org/10.1007/s42114-022-00434-1>
- [51] J. Marzbanrad, M. Akbari, P. Asadi, S. Safaee. Characterization of the influence of tool pin profile on microstructural and mechanical properties of friction stir welding. *Metallurgical and Materials Transactions B* **45**(5):1887–1894, 2014. <https://doi.org/10.1007/s11663-014-0089-9>

- [52] M. K. Gupta. Effects of tool profile on mechanical properties of aluminium alloy Al 1120 friction stir welds. *Journal of Adhesion Science and Technology* **34**(18):2000–2010, 2020. <https://doi.org/10.1080/01694243.2020.1749448>
- [53] Z. Ma, Q. Li, L. Ma, et al. Process parameters optimization of friction stir welding of 6005A-T6 aluminum alloy using Taguchi technique. *Transactions of the Indian Institute of Metals* **72**(7):1721–1731, 2019. <https://doi.org/10.1007/s12666-019-01639-7>
- [54] K. Elangovan, V. Balasubramanian. Influences of pin profile and rotational speed of the tool on the formation of friction stir processing zone in AA2219 aluminium alloy. *Materials Science and Engineering: A* **459**(1):7–18, 2007. <https://doi.org/10.1016/j.msea.2006.12.124>
- [55] M. H. Shojaeefard, M. Akbari, A. Khalkhali, et al. Optimization of microstructural and mechanical properties of friction stir welding using the cellular automaton and Taguchi method. *Materials & Design* **64**:660–666, 2014. <https://doi.org/10.1016/j.matdes.2014.08.014>
- [56] K. Elangovan, V. Balasubramanian. Influences of tool pin profile and welding speed on the formation of friction stir processing zone in AA2219 aluminium alloy. *Journal of Materials Processing Technology* **200**(1):163–175, 2008. <https://doi.org/10.1016/j.jmatprotec.2007.09.019>